# A colorimetric detection of microRNA-148a in gastric cancer by gold nanoparticles-RNA conjugates

To cite this article before publication: Jun Cai *et al* 2019 *Nanotechnology* in press https://doi.org/10.1088/1361-6528/ab55b7

# A colorimetric detection of microRNA-148a in gastric cancer by gold nanoparticles-RNA conjugates

Jun Cai, Liyun Ding*, Panfeng Gong, Jun Huang

National Engineering Laboratory for Fiber Optic Sensing Technology, Wuhan University of Technology, Wuhan, 430070, China

*dlyw@whut.edu.cn

**Abstract:** For the early diagnosis of gastric cancer, microRNA-148a as a promising biomarker is measured by a simple colorimetric biosensor due to the unique surface plasmon resonance (SPR) absorption of gold nanoparticles (AuNPs). In the assay system, the sensing probes are facilitated by the conjugation of AuNPs with RNA probes ($RNA_P$) vis Au-S bond, which align in a tail-to-tail fashion onto the target RNA. When miRNA-148a is introduced, the sandwich hybridization reaction is triggered between the AuNPs-$RNA_P$ conjugates and targets, resulting in changes in SPR absorption band, microscopic distribution and macroscopic color of the AuNPs solution. Following the principle, this colorimetric method is able to quantitatively detect miRNA-148a at nanomolar level with a limit of ~1.9 nM and exhibits high sensitivity and selectivity by a low-cost UV-Vis spectrometer or even naked eye. Moreover, the AuNPs network materials with a characteristic sharp "melting transition" provide significant guidance for the reusability of DNA or RNA biosensor.

**Keywords:** AuNPs-$RNA_P$ conjugates, SPR absorption, miRNA, gastric cancer

## 1. Introduction

Gastric cancer, as one of the most common malignant disease, is the second leading cause of cancer-related death worldwide [1]. The improvement of clinical diagnosis and treatment can result in a relatively high survival rate for patients with early-stage gastric cancer, while the prospect of patients with advanced gastric cancer are still poor [2]. Therefore, early diagnosis and prognosis monitoring are very critical to prevent the death from gastric cancer [3].

Currently, emerging evidences have demonstrated that microRNAs (miRNAs) can be as a promising biomarker for the diagnosis of gastric cancer [4,5]. The miRNAs, composed of 19-25 nucleotides, are small non-protein-coding RNAs which play an important role in regulating gene expression at transcription and post-transcription level [6]. Some certain miRNAs are expressed abnormally in many kinds of cancers, in which deregulated miRNAs are associated with tumor initiation, promotion, and progression by regulating various oncogenes or tumor suppressors [6-8]. A downregulation of miRNAs is common in human cancers, and miRNAs loss may lead to a tumor initiation [9,10]. In the case of gastric cancer, miRNA-148a is one of the most downregulated miRNAs in patient plasma [11-15]. These facts support that miRNA-148a can be served as a prognostic biomarker for gastric cancer, however, a reliable biosensor for miRNA-148a is still rare. Thusly, it is necessary to provide minimally invasive detection for releasing the human health issues of cancer by the development of bioassay technologies for miRNAs in plasma.

For the detection of miRNAs, a variety of approaches have been studied such as electrical, mass, and optical sensors with the aid of micro-electro-mechanical systems as well as nanotechnology [16-19]. More traditional and widely used methods such as polymerase chain reaction (PCR) can measure the promising biomarker miRNA but they still have many limitations with a relatively low sensitivity [20]. Especially, PCR technique requires the time-consuming and large power equipment, which means comparatively high cost [21]. Among the different sensing systems available, a colorimetric assay has been widely used for in DNA or RNA for the reason that this method has not only excellent sensitivity, specificity and reproducibility but also low-

cost and easy operation [22-28]. A colorimetric sensor is usually used for analyzing through the change of absorbance and even the visual color. The signal-conversion element is extremely critical to design a feasible colorimetric biosensor, and nanomaterials like gold nanoparticles (AuNPs) play important roles in the present sensor technologies. The AuNPs possess a unique optical property with surface plasmon resonance (SPR), induced by the collective oscillation of free electrons resonated with the incident photon frequency [29-31]. Importantly, the SPR absorption band of AuNPs varies with the microscopic distribution state of the nanoparticles converting from dispersion to aggregation, and a macroscopic change of appearance color occurring simultaneously [31]. Therefore, the AuNPs are commonly employed in colorimetric assays.

In the present study, we develop a simple and low-cost colorimetric assay to quantitatively detect miRNA-148a concentration using AuNPs conjugated with RNA as sensing probes. The conjugation of oligonucleotides to AuNPs allows convenient modification of the nanoparticle surfaces and precise control of the particle distribution state (dispersed/aggregated) through sandwich hybridization reaction between the conjugated probes and target RNA. Meanwhile, the SPR absorption peak, microscopic distribution and macroscopic color of the AuNPs solution will change. It makes the measurement of miRNA-148a more available by UV-Vis spectrometer or even naked eye.

## 2. Materials and methods

### 2.1 Chemicals and apparatus

Gold(III) chloride trihydrate ($HAuCl_4 \cdot 3H_2O$), trisodium citrate, Tris(2-carboxyethyl)phosphine hydrochloride (TCEP), sodium chloride (NaCl) and sodium dodecyl sulfate(SDS) are bought from Aladdin Industrial Co. sodium phosphate dibasic dehydrate ($Na_2HPO_4 \cdot 2H_2O$), sodium dihydngen phoshate anhydrous ($NaH_2PO_4$), ethanol, $HNO_3$ (68%) and HCl (38%) are purchased from Sinopharm Chemical Reagent Beijing Co. Ltd. All the chemicals are analytical grade. All procedures were performed at room temperature if not specially noted. Ultra-pure (U-P) water was produced by the Hitech-K flow water purification system.

RNA oligonucleotides were obtained from Shanghai Sangon Biotechnology Co. Ltd. The RNA base sequences are summarized in Table 1. Following the manufacturer's recommendations, all the RNA sequences were dissolved in nuclease-free water prior to use.

The UV-vis absorbance spectra and TEM images of samples performed on the UV-2450 spectrometer (Shimadzu, Japan) and JEM-2100 transmission electron microscope (JEOL, Japan) operating at 200 kV, respectively.

**Table 1**

RNA sequences used in colorimetric detection

| Name | Sequence (5'-3') |
|---|---|
| miRNA-148a | UCAGUGCACUACAGAACUUUGU |
| Probe 1 | UAGUGCACUGACCCC－SH |
| Probe 1' | HS－CCCCUAGUGCACUGA |
| Probe 2 | HS－CCCCACAAA GUUCUG |
| miRNA-21 | UAGCUUAUCAGACUGAUGUUGA |
| miRNA-106a | AAAAGUGCUUACAGUGCAGGUAG |
| random | UUGUACUACACAAAAGUACUG |

**2.2 Preparation of AuNPs**

Approximately 22 nm diameter AuNPs were synthesized by the trisodium citrate reduction of gold chloride, as previously reported [32]. All glassware used in the experiment was cleaned with aqua regia (1 part $HNO_3$ and 3 parts HCl), rinsed with U-P water, and then dried by an oven prior to use. An aqueous solution of $HAuCl_4$ (0.01% (w/w), 50 mL) was heated to boiling, and then trisodium citrate (1% (w/w), 880 μL) was added quickly, resulting in a change of solution color from pale yellow to wine red. After the color change, the reaction solution was boiled for additional 20 minutes, allowed to cool to room temperature and then stored at 4 ℃. Attentively, constant stirring was maintained throughout the process of preparation in order to keep the reaction solution heated uniformly. TEM was used to determine the size and dispersity of prepared nanoparticle solutions and UV-Vis spectrometer was selected to record the absorbance spectra to calculate the concentration and size of AuNPs [33, 34].

### 2.3 Preparation of AuNPs-RNA$_P$ conjugates

The conjugation of AuNPs modified with thiolated RNA probes (RNA$_P$) was prepared based on the salt aging procedures proposed by Mirkin et al [35]. Firstly, a total of 5 mL AuNPs (22 nm) colloid was centrifuged and the obtained precipitate was redispersed in PBS buffer (10mM $Na_2HPO_4$, and $NaH_2PO_4$, 0.01% (w/w) SDS, pH=6.8). Freshly prepared TCPE (10 mM) diluted in nuclease-free water was added to RNA (probe 1, 1' or 2) solution to prevent the formation of disulfide bonds generated at the thiolated end of RNA. Then a certain volume of RNA solution (20 μM) and AuNPs colloid (~1 nM) were incubated at the molar ratio of 200:1 and 600: 1 for 12 h. After that, a tiny amount of 2 M NaCl solution was added to the mixture to increase gradually the salt concentration, and then the solution was sonicated for ~10 s followed by an 1-h incubation period. This process was repeated for several times till a concentration of 0.1 M NaCl was obtained. The resultant solution was incubated for another ~24 h and then centrifuged at 12000 rpm for 20 min to remove excess unconjugated RNA. Following the removal of supernatant by a pipette, the oily precipitate was washed with the buffer (10mM $Na_2HPO_4$, and $NaH_2PO_4$, 0.01% (w/w) SDS, 0.1 M NaCl, pH=6.8), centrifuged again, resuspended in hybridization buffer (10mM $Na_2HPO_4$, and $NaH_2PO_4$, 0.01% (w/w) SDS, 0.3 M NaCl, pH=6.8). If not otherwise specified, the entire incubation process was performed at room temperature while stirring ceaselessly. Finally, the UV-Vis spectrometer device were used to test whether the RNA was conjugated with the surface of AuNPs.

### 2.4 Measurement of microRNA-148a detection

In order to determine the sensitivity and the limit of detection (LOD), AuNPs-RNA$_P$ conjugates/target miRNA-148a solutions was prepared by adding 50 μL miRNA-148a solution (with its final concentration ranging from 0.1 nM to 1 μM in the increase of 10 times) to a mixture solution containing 225 μL of each AuNPs-RNA$_P$ conjugates at hybridization buffer. After that, the mixture solutions were heated to 60 ℃ for 5 min and cooled down to room temperature, then incubated for a period. The same assay was used to test the selectivity by replacing the target RNA with other

different sequences at a certain concentration of 1 μM. The UV-Vis signature of the AuNPs-RNA conjugates/miRNA-148a aggregates was recorded at room temperature.

**2.5 Melting analyses**

Melting experiments were performed using a UV-Vis spectrometer equipped with a temperature controller by monitoring the absorbance at wavelength 530 nm. The AuNPs-$RNA_P$ conjugates/target RNA solutions were prepared according to the aforementioned method with the miRNA-148a concentration of 1 μM. After 5 min of annealing at 60 ℃, the samples were cooled down to room temperature for more than 2 h before analysis. The solutions were agitated by shaking intermittently the cuvette to remain homogeneous throughout the melting process.

**3 Results and discussion**

**3.1 Method and principle**

As shown in Fig. 1, the assembly of the AuNPs converting from dispersed to aggregated state is controlled in the presence of target RNA due to the sandwich hybridization between AuNPs-$RNA_P$ conjugates and targets, accompanied with a macroscopic color change (red-to-purple). Firstly, a highly dispersed AuNPs are prepared with a strong surface plasmon absorption and a responding wine red hue. Those oligonucleotides (RNA probe1 ($RNA_{P1}$) or probe2 ($RNA_{P2}$)) functionalized with thiols at their 3' or 5' termini are easily conjugated to the surface of AuNPs via Au-S bond. After conjugation with the thiol-capped oligonucleotides, the two AuNPs-$RNA_P$ conjugates are mixed together, and no reaction takes place owing to the non-complementary nature of the probe sequences. Nevertheless, when the target miRNA-148a (complementary to the sequences of two kind of probes in a "tail-to-tail" fashion) is added into the mixture solution, the RNA hybridization reaction is triggered, which makes the original dispersed AuNPs develop into aggregated AuNPs. Significantly, because of the aggregation of AuNPs, their interparticle surface plasmons are coupled so that the aggregate could be considered as a single larger particle [31]. As a result, the surface plasmon absorption band of AuNPs solution is broadened and red-shifted, corresponding to the color change from red to purple. Therefore, the different concentration of target RNA can be detected by the UV-Vis absorption spectra and even

naked eye.

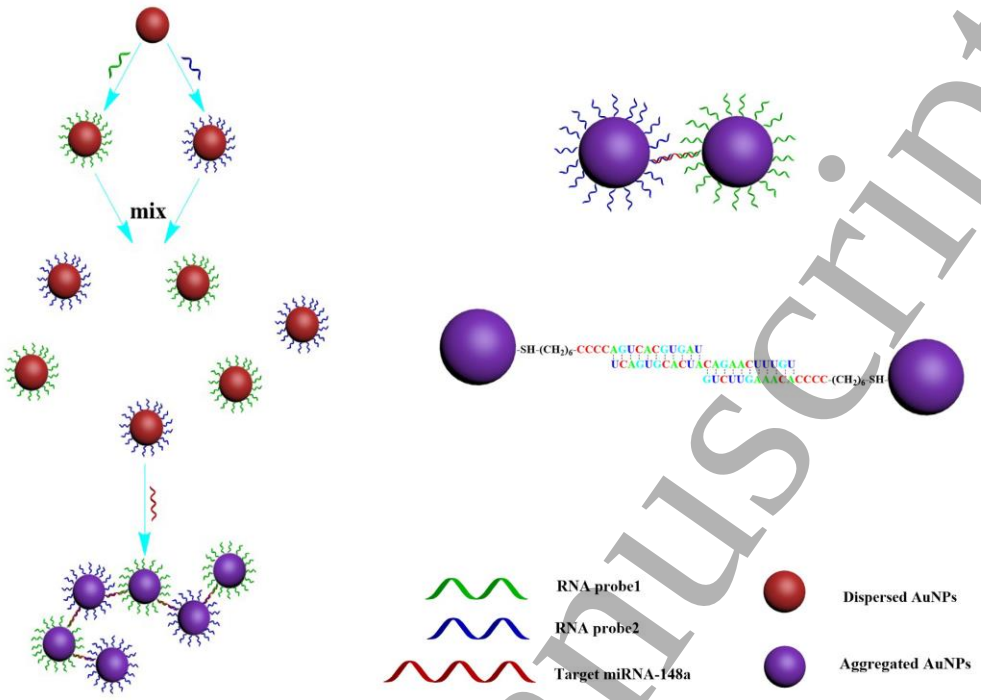


Fig. 1 Schematic illustration of AuNPs-RNA conjugations based colorimetric biosensor for miRNA-148a.

### 3.2 Optic properties and morphology of AuNPs and AuNPs-RNA$_P$ conjugates

The prepared AuNPs were characterized by UV-Vis spectrometer with a typical SPR absorption peak at 525 nm (Fig. 2(a)). The estimated diameter and concentration of the AuNPs are ~22 nm and ~1 nM, respectively [34]. Additionally, the uniformly spherical AuNPs were observed according to TEM images (Fig. 2(b)) and the diameter was obtained around 22 nm using a supplementary graph software, which was in accordance with the calculated results from UV-Vis spectra. The AuNPs were chemically modified with thiol-capped 15-base RNA$_P$, in which the first 4 nucleotides (CCCC) served as a flexible spacer, and the last 11 nucleotides served as a recognition element for the target RNA. The accurate number of RNA$_P$ attached to each individual AuNP has not yet been determined, but many RNA$_P$ molecules conjugated to each AuNP are confirmed (vide infra). The UV-vis spectra of bare AuNPs and AuNPs-RNA$_P$ conjugates are shown in Fig. 3. After modification with RNA$_P$, a modest red-shift from 525 to 530 nm and intensity reduction in the SPR absorption peak were observed which indicated the successfully conjugation of RNA$_P$ on the AuNPs [37]. As the diameter of

AuNPs (~22nm) has been determined, the molar extinction coefficient at 450 nm ($\varepsilon_{450}$) of nanoparticle is about $7.31\times10^{8}$ ($M^{-1}cm^{-1}$) [34]. Based on the Lambert Beer law, the nanoprobe concentration can be calculated by the formula ($c = A_{450}/\varepsilon_{450}$) for a standard path length of 1 cm. Hence, we obtained the concentration of AuNPs-RNA$_{P1}$ and AuNPs-RNA$_{P2}$ conjugates about 790 pM and 810 pM, respectively.

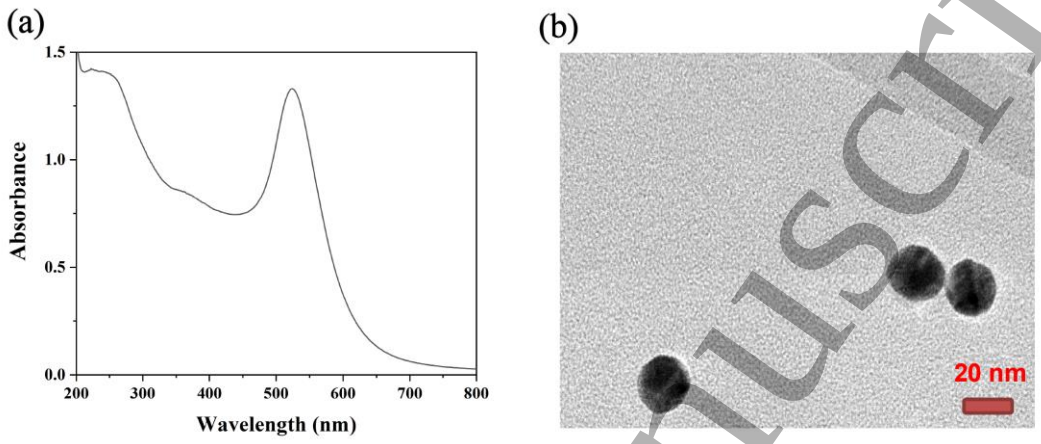


Fig. 2. (a) UV-vis absorption spectra of the AuNPs and (b) TEM image of the AuNPs.

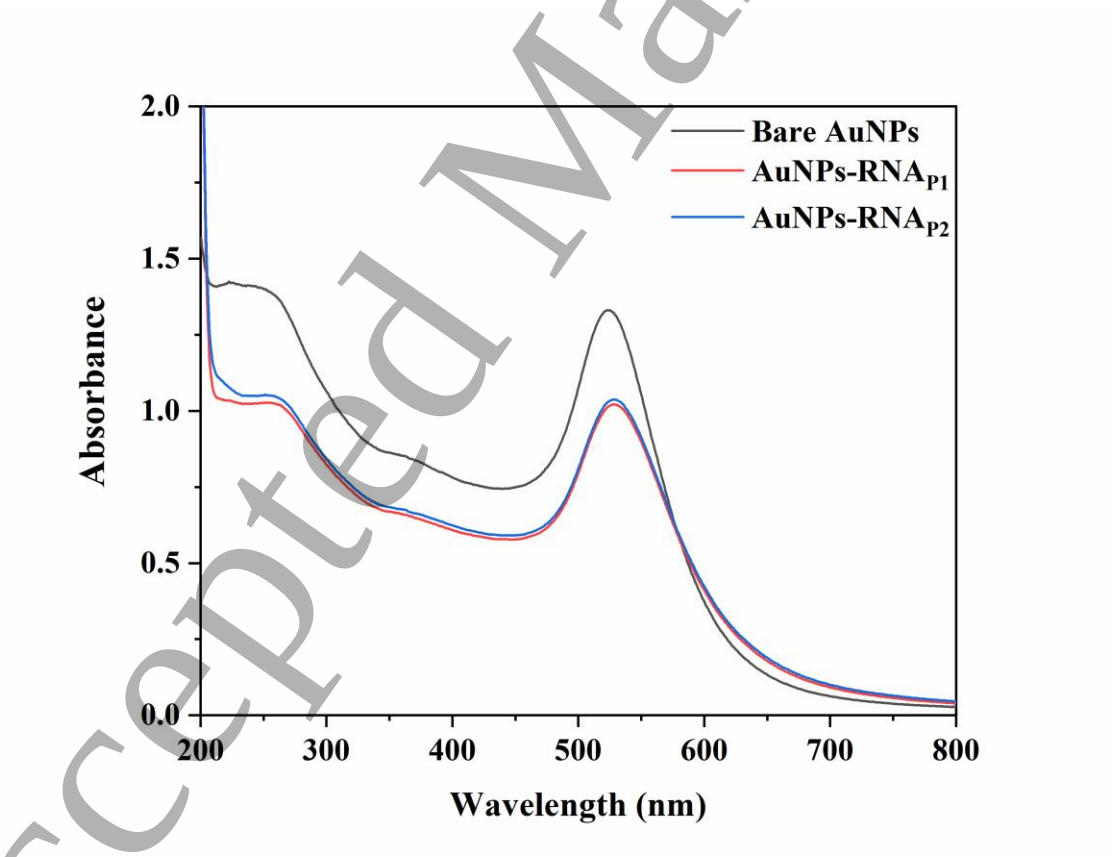


Fig. 3. Comparison of UV-Vis spectra for bare AuNPs and AuNPs-RNA$_P$ conjugates.

To verify the principle, we prepared a colorimetric assay based on AuNPs-RNA$_P$ conjugates as mentioned above. An equal volume of test solution containing 0 or 1 μM

target RNA was added into the mixed AuNPs-RNA$_P$ solutions for hybridization reaction. In the absence/presence of miRNA-148a, the UV-Vis absorption spectra and relative TEM images were displayed in the Fig. 4, respectively. When miRNA-148a absents, the SPR absorption peak of the mixture solution appears no significant change at 530 nm (Fig. 4(a), black line) and its color maintains wine red with a good dispersion observed by TEM (Fig. 4(b), inset centrifuge tube and corresponding TEM image, left). In contrast, when 1 μM miRNA-148a presents, the intensity of SPR absorption peak weakens dramatically with a redshift from 530 to 568 nm wavelength (Fig. 4(a), red line). Meanwhile, the microscopic distribution of AuNPs changes obviously from original dispersion to aggregation and its macroscopic color turns to a purple hue (Fig. 4(b), inset centrifuge tube and corresponding TEM image, right).

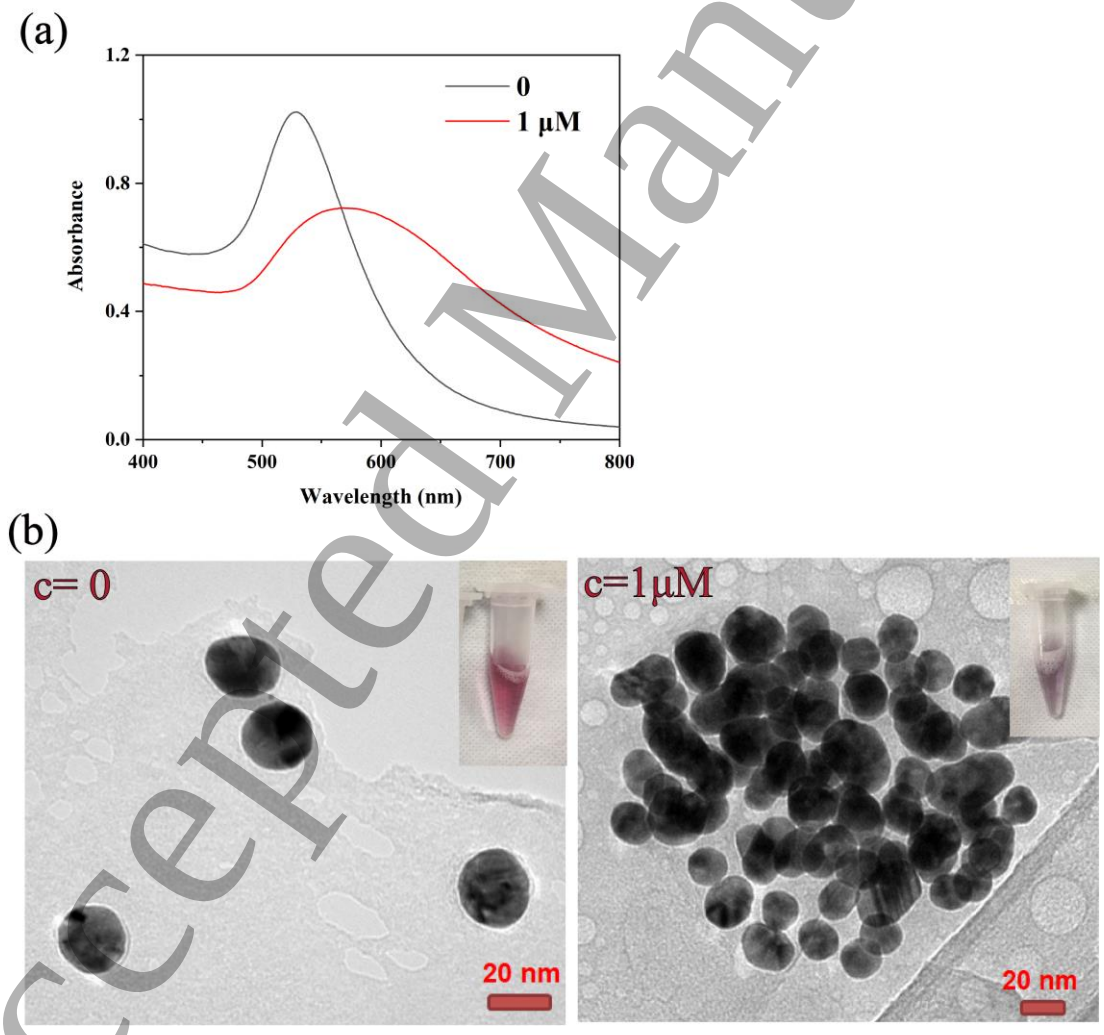


Fig. 4(a) Comparison of UV-Vis spectra for AuNPs-RNA$_P$ conjugates solution in the absence/presence of miRNA-148a. (b) TEM images and corresponding real photographs of complementary bases in the presence of 0 (left) and 1 μM (right) target miRNA-148a.

### 3.3 Optimization of conditions

Single-stranded thiolated oligonucleotides can be chemically attached to citrate capped AuNPs, resulting in increased stability of gold colloid, which promises the basis of biochemical analyses and applications [38]. With the protection of the $RNA_P$, these modified AuNPs can sustain stability even in solution containing high salt concentration (0.3M NaCl), an environment that is incompatible with unmodified AuNPs [37, 38]. However, the AuNPs-$RNA_P$ conjugates with a relative low ratio of $RNA_P$ to AuNPs (200:1) collapsed completely once resuspensed in hybridization buffer. When the ratio increased to 600:1, the conjugates were still able to maintain stability in the high salt buffer (Fig. 5). Obviously, the stability of AuNPs-$RNA_P$ conjugates is dependent on the ratio of RNA to AuNPs. The high ratio can guarantee that enough $RNA_P$ were conjugated to AuNPs, providing the conjugates with a higher stability in high salt solution, presumably because these abundant non-complementary $RNA_P$ conjugated to the surface with a higher stability can prevent them from collapsion. Hence, the $RNA_P$:AuNPs at a ratio of 600:1 was used in the following salting experiments.

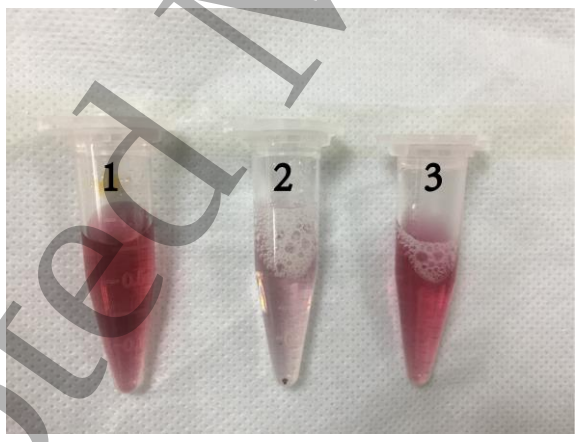


Fig. 5. Pictures of different ratio of $RNA_P$ to AuNPs. The sample 1 is the original AuNPs solution without modification; the sample 2 is the conjugates at a ratio of 200:1 in hybridization buffer; the sample 3 is the conjugates at a ratio of 600:1 in hybridization buffer. These pictures clearly show the collapsion of the conjugates at a relative low ratio in hybridization buffer.

The alignment fashion of AuNPs probes may play a significant role in determining the degree of hybridization reaction between complementary bases due to the steric consideration [35, 39]. In the presence of 1 μM target miRNA-148a, the UV-Vis absorption spectra and relative pictures of AuNPs-$RNA_P$ conjugates by the "Tail-to-

Tail (TT)" or "Head-to-Tail (HT)" alignment were shown in the Fig. 6(a) and (b), respectively. When AuNPs probes (1 and 2) align in a TT fashion onto the complementary target miRNA, the hybridization reaction takes place normally. However, the reaction cannot happen effectively by the HT alignment between the AuNPs probes (1' and 2) and miRNA-148a, which can be owing to the steric hindrance. Although it is difficult to obtain the exact length of RNA, the whole relative size of RNA probes (5.1 nm) and target (7.48 nm) is estimated from the base pairs (bp) with a distance of 0.34 nm/bp in the current researches [39, 40], and its relative size is depicted in Fig. 6(c). The AuNPs are very likely to collide when the AuNPs-RNA$_P$ conjugates align in a HT fashion, which accounts for the ineffective hybridization reaction. Thus, the alignment in TT fashion between AuNPs-RNA$_P$ conjugates and complementary target is selected in the following assays.

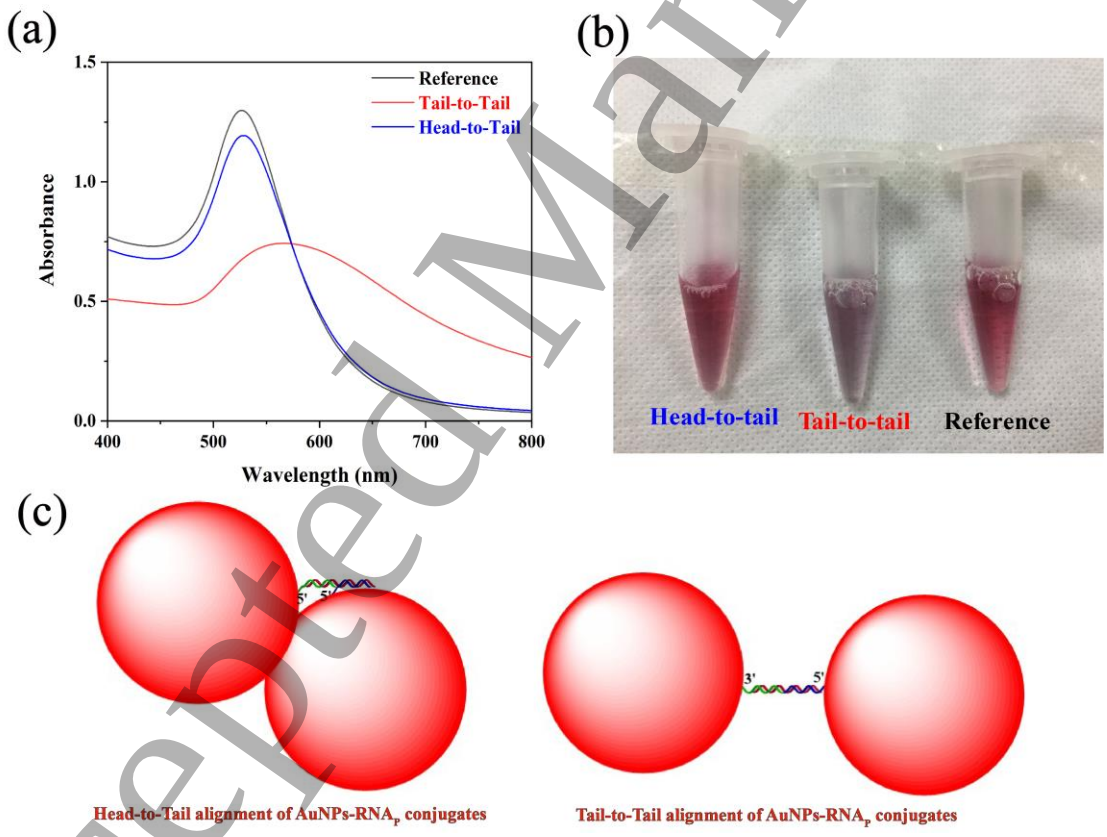


Fig. 6. (a) Comparison of UV-Vis spectra and (b) corresponding pictures for AuNPs-RNA$_P$ conjugates solution by the tail-to-tail or head-to-tail alignment in the presence of 1 μM miRNA-148a. The reference is only AuNPs-RNA$_P$ conjugates without miRNA-148a. (c) Relative size of RNA and AuNPs. The left and right represents the conjugates aligns in a HT and TT fashion, respectively.

To assess the response time of the assay, the solution with the miRNA-148a concentration of 1 μM was used to detect. After the target RNA was added into the solution containing two kinds of AuNPs-$RNA_P$ conjugates, the mixture was heated for the promotion of hybridization reaction. And then the mixture was naturally cooled down to the room temperature, which costed about 15 min. Finally, we tested the UV-vis spectra of the samples with an interval of 5 min. The solution was agitated by shaking the vessel to maintain homogeneous mixtures throughout the detection period. The absorbance of reaction solution at 530 nm changes and becomes stable about 80 min as plotted in Fig. 7. In addition, we also found that the color of the mixture solution roughly unchanged at the same time. Therefore, based on the UV-Vis spectra and color change of the mixture, we waited for about 100 min (including 5min heating, 15 min cooling, and 80 min incubation process) before taking a measurement for each assay.

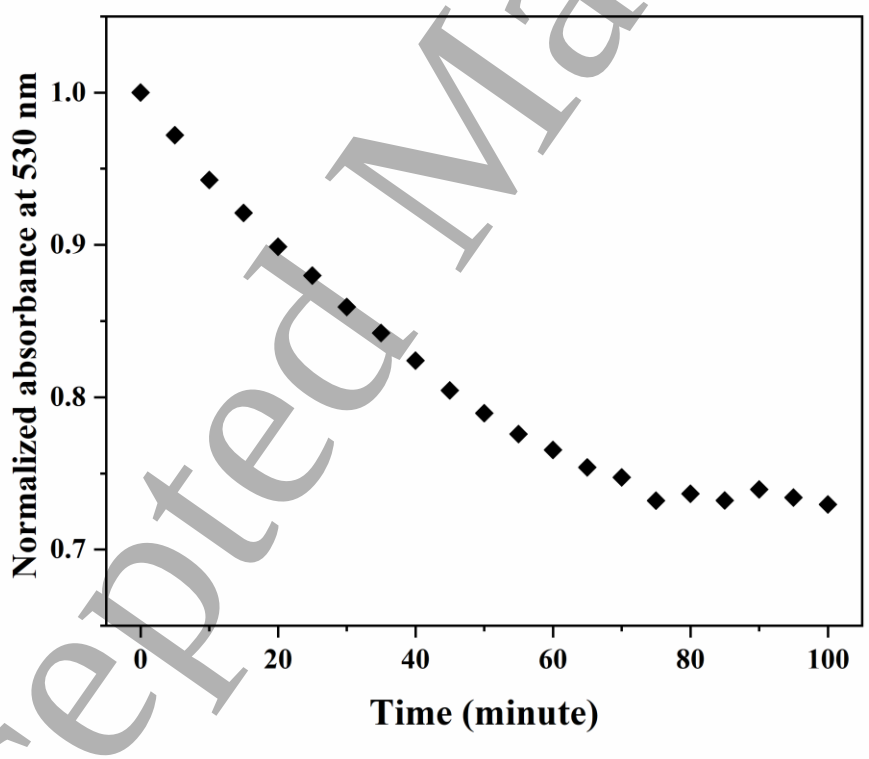


Fig. 7. Response time by monitoring the absorbance at 530 nm.

### 3.4 RNA hybridization assay for the detection of miRNA-148a

To evaluate the detection capability of the colorimetric biosensor, we have to determine the LOD and dynamic range of this biosensor. Fig. 8(a) gives the UV-Vis

absorption spectra and visual colors of the detection system with different concentration of target miRNA-148a. Obviously, when the concentration of miRNA-148a reaches 1 μM the corresponding UV-Vis spectrum appears a new sharp absorption at 260 nm resulting from the excessive miRNA-148a [41, 42], which means that the detectable concentrations reached a saturation point. The quantitative analysis of miRNA-148a, with concentration ranging from 0.1 nM to 1 μM in the increase of 10 times, was employed. The tendency for ΔA in presence of miRNA-148a is depicted in Fig. 8(b), in which ΔA is the difference value for SPR peak absorbance of AuNPs-RNA$_P$ conjugates solution in absence and presence of miRNA-148a, and the lower value means that the less aggregation occurred. When the low concentration ranging to 0.1 nM level of miRNA-148a is added into the mixture probe solutions, the ΔA is almost zero. This level of concentration is too low to develop a sandwich hybridization between the AuNPs-RNA$_P$ conjugates and miRNA-148a. Moreover, the LOD was estimated approximately 1.9 nM by 3 signal-to-noise ratio (20 times determinations of the blank solution). This method exhibited a lower LOD than recently reported other assays [20,23]. Additionally, as the concentration of miRNAs in plasma is up to ~nM, the change of the SPR absorption peak absorbance can be meaningful for clinical application.

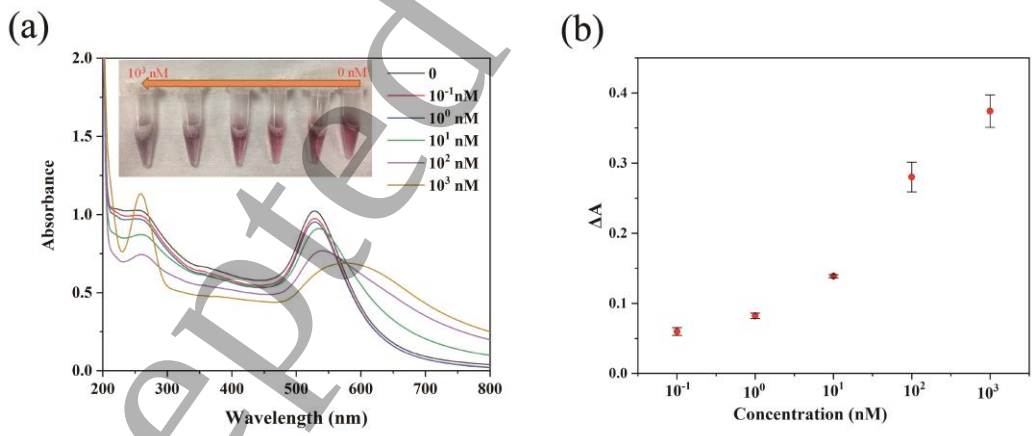


Fig. 8. (a) UV-Vis spectra and visual colors of the AuNPs-RNA$_P$ conjugates based colorimetric detection in presence of different concentration of miRNA-148a. (b) ΔA change corresponding to the miRNA-148a concentration ranging from $10^{-1}$ nM to $10^3$ nM by 10 times.

### 3.5 Selectivity of the colorimetric detection

For the clinical application of our sensing system, it is necessary to verify the

specificity in the assay of target miRNA-148a. The other several samples of miRNA-21, miRNA-106a, random sequences were prepared to estimate the selectivity of this method for miRNA-148a detection. 1 μM each RNA samples were added to the mixed AuNPs-RNA$_P$ conjugates solution respectively, and the AuNPs-RNA$_P$ solution without any miRNA was tested as blank assay. The results of experiment were shown in Fig. 9. Obviously, we could find that these other RNA samples were unable to trigger the hybridization reaction, and only the target miRNA-148a gave rise to the aggregation of AuNPs, which was confirmed by the variations of absorbance (Fig. 9(a)) and color changes (Fig. 9 (b)). Compared with other RNA, the ΔA changes significantly in presence of target RNA, indicating that the proposed method has highly selectivity to miRNA-148a detection.

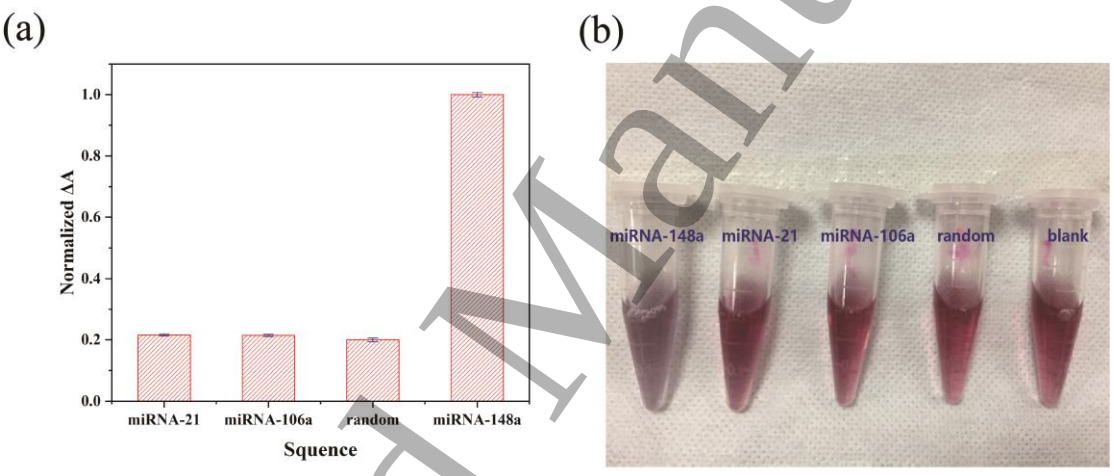


Fig. 9. Specificity of the colorimetric detection for miRNA-148a against other RNA sequences: (a) the difference of absorbance and (b) color changes.

### 3.6 Melting point

In order to find the melting point ($T_m$) of the aggregates quickly and efficiently, the $T_m$ was estimated roughly about 50 ~ 60 ℃ by the color change of sample solution at different temperatures (ranging from 30 ℃ to 60 ℃ in the increase of 10 ℃, shown in Fig. 10(a)), and then measured accurately by the UV-Vis absorption spectra of the solution at the obtained temperature region with an interval of 1 ℃. The normalized thermal dissociation curve for AuNPs-RNA$_P$ conjugates with complementary target RNA in hybridization buffer was shown Fig. 10(b). A characteristic sharp melting transition was observed with a $T_m$ of ~54 ℃, indicating the dissociation of aggregated

AuNPs and formation of dispersed nanoparticles. This sharp melting transition brings a new possibility for the reusability of DNA or RNA biosensor by heating the AuNPs network materials to a temperature slightly higher than $T_m$ when one kind of AuNPs-$RNA_P$ conjugates is immobilized on a proper substrate.

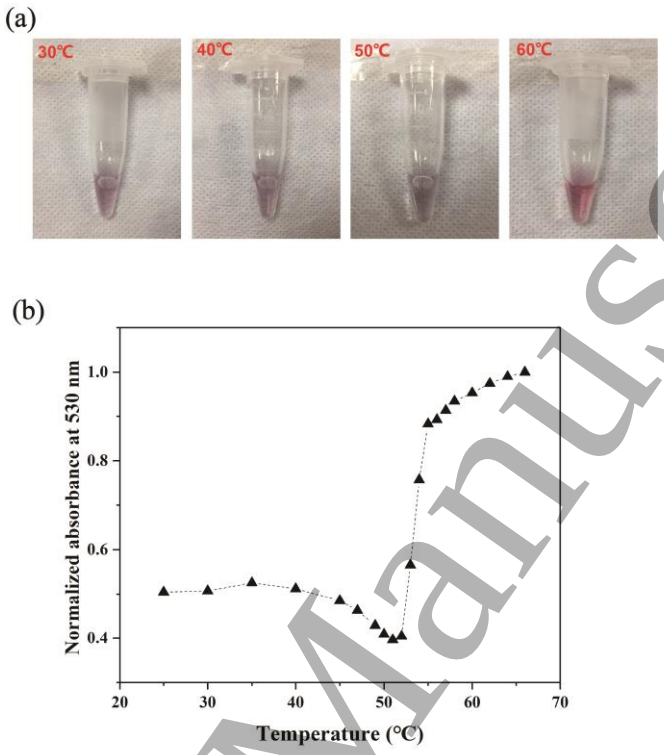


Fig. 10 (a) The color of aggregates under different temperature. (b) The melting curve of the aggregates in hybridization buffer by monitoring the absorption at 530 nm.

## 4. Conclusion

In summary, we have developed a simple and low-cost colorimetric method for quantitative detection of miRNA-148a with high sensitivity and specificity. This assay is following the principle that the sandwich hybridization reaction takes place between the AuNPs-$RNA_P$ conjugates and targets by the "tail-to-tail" alignment in the presence of target RNA, which results in changes in SPR absorption peak, microscopic distribution and macroscopic color of the AuNPs solution. Under the optimized conditions, the proposed colorimetric biosensor can detect miRNA-148a down to the limit of ~1.9 nM concentration, which can be utilized for the early detection of gastric cancer. Additionally, the sharp melting transition of AuNPs network materials provides significant guidance for the reusability of DNA or RNA biosensor. This methodology may offer a universal approach to the detection of base sequences in biological filed.

**Acknowledgment**

This work is supported by Financial Support from the National Natural Science Foundation of China (NO. 51878524, NO. 61575150).

## References


[1] Parkin D M, Bray M F, Ferlay M J and Pisani P 2005 Global Cancer Statistics, 2002 CA: Cancer J Clin. **55** 74-108

[2] Hohenberger P P and Gretschel S 2003 Gastic cancer Lancet **362** 305–315

[3] Leung W K et al 2008 Screening for gastric cancer in Asia: current evidence and practice Lancet Oncol **9** 279-287

[4] Paranjape T, Slack F J and Weidhaas J B 2009 MicroRNAs: tools for cancer diagnostics Gut **58** 1546-1554

[5] Ding J et al 2010 Gain of miR-151 on chromosome 8q24.3 facilitates tumour cell migration and spreading through downregulating RhoGDIA Nat. Cell Biol. **12** 390-399

[6] Bartel D P 2004 MicroRNAs: genomics, biogenesis, mechanism, and function Cell **116** 281–97

[7] Calin G A and Croce C M 2006 MicroRNA signatures in human cancers Nat. Rev. Cancer **6** 857–66

[8] Esquela-Kerscher A and Slack F J 2006 Oncomirs: microRNAs with a role in cancer Nat. Rev. Cancer **6** 259–69

[9] Kumar M S et al 2007 Impaired microRNA processing enhances cellular transformation and tumorigenesis Nat. Genet. **39** 673-677

[10] Lu J et al 2005 MicroRNA expression profiles classify human cancers Nature **435** 834-838

[11] Ueda T et al 2010 Relation between microRNA expression and progression and prognosis of gastric cancer: a microRNA expression analysis Lancet Oncol. **11** 136-146

[12] Zheng B Q et al 2011 MicroRNA-148a Suppresses Tumor Cell Invasion and Metastasis by Downregulating ROCK1 in Gastric Cancer Clin. Cancer Res. **17** 7574-7583

[13] Goedeke L et al 2015 MicroRNA-148a regulates LDL receptor and ABCA1 expression to control circulating lipoprotein levels Nat. Med. **21** 1280–1289

[14] Sakamoto N et al 2014 MicroRNA-148a is downregulated in gastric cancer, targets MMP7, and indicates tumor invasiveness and poor prognosis Cancer Sci. **105** 236-243

[15] Idichi T et al 2018 Molecular pathogenesis of pancreatic ductal adenocarcinoma:Impact of passenger strand of pre-miR-148a on gene regulation Cancer Sci. **109** 2013-2026

[16] Wang Z, Si L, Bao J and Dai Z 2015 A reusable microRNA sensor based on the electrocatalytic property of heteroduplex-templated copper nanoclusters Chem. Commun. **51** 6305–6307

[17] Johnson B N and Mutharasan R 2014 Biosensor-based microRNA detection: techniques, design, performance, and challenges Analyst **139** 1576–1588

[18] Li M, Cushing S K and Wu N 2015 Plasmon-enhanced optical sensors: a review Analyst **140** 386–406

[19] Park S H, Lee J and Yeo J S 2018 On-chip plasmonic detection of microRNA-106a in gastric cancer using hybridized gold nanoparticles Sensors Actuat. B: Chem. **262** 703-709

[20] Klein D 2002 Quantification using real-time PCR technology: applications and limitations Trends Mol. Med. **8** 257–260

[21] Riedel T E et al 2014 Detection limits and cost comparisons of human- and gull-associated conventional and quantitative PCR assays in artificial and environmental waters J. Environ. Manage. **136** 112-120

[22] Sattarahmady N et al 2015 Gold nanoparticles biosensor of Brucella spp. genomic DNA: Visual and spectrophotometric detections Bioche. Eng. J. **97** 1-7

[23] Kao H W et al 2014 Biological characterization of cetuximab-conjugated gold nanoparticles

ina tumor animal model Nanotechnology **25** 295102

[24] Zhan Z R, Ma X Y, Cao C and Sim S J 2012 Gold-based optical biosensor for single-mismatched DNA detection using salt-induced hybridization Bisens. Bioelectron. **32** 127-132

[25] Xu C N, Lan L Y, Yao Y, Ping J F, Li Y B and Ying Y B 2018 An unmodified gold nanorods-based DNA colorimetric biosensor with enzyme-free hybridization chain reaction amplification Sensors Actuat. B: Chem. **273** 642-648

[26] Valentini P, Fiammengo R, Sabella S, Gariboldi M, Maiorano G, Cingolani R and Pompa P P 2013 Gold-Nanoparticle-Based Colorimetric Discrimination of Cancer-Related Point Mutations with Picomolar Sensitivity ACS Nano **7** 5530-5538

[27] Hong L, Lu M, Dinel M P, Blain P, Peng W, Gu H and Masson J 2018 Hybridization conditions of oligonucleotide-capped gold nanoparticles for SPR sensing of microRNA Bisens. Bioelectron. **109** 230-236

[28] Li H X and Rothberg L 2005 Detection of Specific Sequences in RNA Using Differential Adsorption of Single-Stranded Oligonucleotides on Gold Nanoparticles Anal. Chem. 77 6229-6233

[29] Kim J H, Chung C H and Chung B H 2013 Colorimetric detection of UV light-induced single-strand DNA breaks using gold nanoparticles Analyst **138** 783-786

[30] Daniel M C and Astruc D 2004 Gold Nanoparticles: Assembly, Supramolecular Chemistry, Quantum-Size-Related Properties, and Applications Toward Biology, Catalysis, And Nanotechnology Chem. Rev. **104** 293-346

[31] Ghosh S K and Pal T 2007 Interparticle Coupling Effect on the Surface Plasmon Resonance of Gold Nanoparticles: From Theory to Applications Chem. Rev. **107** 4797-4862

[32] Frens G 1973 Controlled Nucleation for the Regulation of the Particle Size in Monodisperse Gold Suspensions Nat. Phys. Sci. **241** 20-22

[33] Grabar K C, Freeman R G, Hommer M B and Natan M J 1995 Preparation and Characterization of Au Colloid Monolayers Anal. Chem. **67** 735-743

[34] Haiss W, Thanh N T K, Aveyard J and Fernig DG 2007 Determination of Size and Concentration of Gold Nanoparticles from UV-Vis Spectra Anal. Chem. **79** 4215-4221

[35] Elghanian R 1997 Selective Colorimetric Detection of Polynucleotides Based on the Distance-Dependent Optical Properties of Gold Nanoparticles Science **277** 1078-1081

[36] Storhoff J J, Elghanian R, Mucic R C, Mirkin C A and Letsinger R L 1998 One-Pot Colorimetric Differentiation of Polynucleotides with Single Base Imperfections Using Gold Nanoparticle Probes J. Am. Chem. Soc. **120** 1959-1964

[37] Giljohann D A, Seferos D S, Daniel W L, Massich M D, Patel P C and Mirkin C A 2010 Gold Nanoparticles for Biology and Medicine Angew. Chem. Int. Edit. **49** 3280-3294

[38] Zhang X, Servos M R and Liu J 2012 Surface Science of DNA Adsorption onto Citrate-Capped Gold Nanoparticles Langmuir **28** 3896-3902

[39] Watson J D and Crick F H C1953 Molecular Structure of Nucleic Acids: A Structure for Deoxyribose Nucleic Acid Nature **171** 737-738

[40] Abbondanzieri E A, Greenleaf W J, Shaevitz J W, Landick R and Block S M 2005 Direct observation of base-pair stepping by RNA polymerase Nature **438** 460-465

[41] Engman K C, Sandin P, S. Osborne, Brown T, Billeter M, Lincoln P, Nordén B, Albinsson B and Wilhelmsson L M 2004 DNA adopts normal B-form upon incorporation of highly fluorescent DNA base analogue tC: NMR structure and UV-Vis spectroscopy characterization

Nucleic Acids Res. **32** 5087-5095
[42] Volkov I L, Reveguk Z V, Serdobintsev P Y, Ramazanov R R and Kononov A I 2017 DNA as UV light–harvesting antenna Nucleic Acids Res. **46** 3543-3551